Simulation of Air Entrainment during Mold Filling: Comparison with Water Modeling Experiments

Seyyed Hojjat Majidi and Christoph Beckermann

Department of Mechanical and Industrial Engineering
The University of Iowa, Iowa City, 52242

Abstract

Reoxidation inclusions form during pouring of steel castings as a result of air entrainment. Recently a model was developed by the authors to predict the volumetric air entrainment during pouring. It was found that the velocity, diameter and turbulence intensity of the liquid stream affect the air entrainment rate during pouring. In this study, the developed air entrainment model is validated with water modeling experiments. In the water modeling studies, water was poured using bottom pour, teapot and quadrant ladles. The effects of nozzle opening, head height, pouring rates and pouring basins are simulated. The predictions compare favorably with the experimental measurements. Results indicate that low head height and short pouring time have a beneficial effect on reducing the air entrainment during pouring. In addition, a fully open nozzle and the use of a nozzle extension for bottom pour ladles further reduce the amount of entrained air.

1. Introduction

Reoxidation inclusions are among the most commonly reported defects in steel castings. These inclusions affect the fatigue strength, fracture toughness, and machinability of a casting and may cause rejection of the cast part [1]. Reoxidation inclusions form when the deoxidized steel comes into contact with oxygen during mold filling. Therefore, limiting the exposure of steel to the oxygen is necessary to minimize reoxidation inclusions.

Air entrainment is the major source of reoxidation inclusion formation during pouring of steel castings. In free surface flows, air is entrained once the liquid experiences surface turbulence. Such surface discontinuities are created, for example, by a hydraulic jump (Figure 1a), or a liquid jet plunging into a pool (Figure 1b). A hydraulic jump occurs when a fast moving liquid discharges into a low velocity atmosphere. As shown in Figure 1a, a significant amount of air is entrained at the toe of the jump and further downstream at the recirculation region. For a plunging liquid jet, once the inertial force of the impinging liquid jet overcomes the restraining forces, including surface tension, air is entrained at the intersecting perimeter of the liquid jet and the pool. While several studies have proposed correlations for the entrainment onset based on the Reynolds and Weber numbers [2,3], Ervine et al. [4] showed that the onset of the air entrainment depends on the turbulence level of the liquid jet. For turbulent water jets, air entrainment commences above approximately 1 m s^{-1}.

1

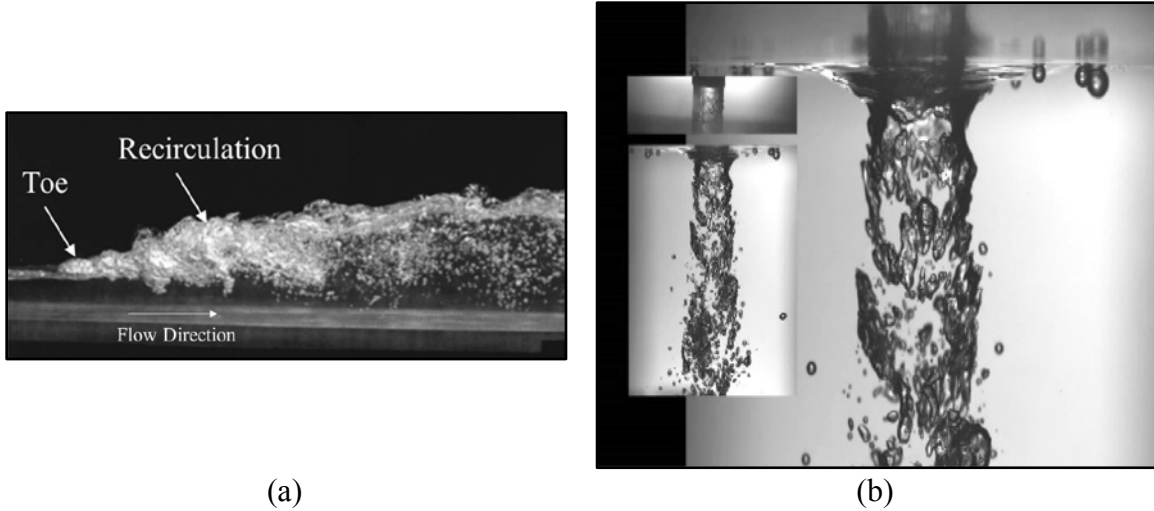|	
(a)	(b)

Figure 1. Air bubbles: (a) in a hydraulic jump, Adapted from "Free Surface Length Scale Estimation in Hydraulic Jumps", by Mouaze et al., 2005 [5], and (b) near a plunging liquid water jet, Reprinted from "Air Entrainment Mechanisms in Plunging Jets and Breaking Waves", by K.T. Kiger and J.H. Duncan, 2012 [6].

Several experiments have been conducted to study the effect of different parameters on the air entrainment for a plunging liquid jet. Based on the results of the measurements, numerous correlations have been proposed for the relative air entrainment rate, Q_a / Q_w, where Q_a and Q_w are the volumetric air entrainment rate and water flow rate, respectively. Experimental studies have shown that the air entrainment depends on the liquid jet velocity at impact, u_j, as: $Q_a / Q_w \propto u_j^n$, where n is a constant. Due to the different experimental conditions and measurement methods, several values of n have been proposed. However, the dependency power, n, has been shown to be in the range of $1.25 \leq n \leq 2$ for liquid jet velocities of $u_j < 6$ m s^{-1} [7-9]. Measurements have also demonstrated that the relative air entrainment increases with an increase in falling height, and decreases with an increase of the liquid jet diameter [4,8,9]. In addition, the turbulence level of the liquid jet has been shown to have a significant effect on the air entrainment rate [4].

In metal castings, the gating system design affects the air entrainment during mold filling. Liquid metal plunging into the sprue and returning waves in the runner are examples of air entrainment in the gating system. The oxygen inside the entrained air reacts immediately with the deoxidized steel to form reoxidation inclusions. These inclusions are then transported with the liquid metal and ultimately end up as non-metallic inclusions in the solidified casting. In steel castings, large reoxidation inclusions often accumulate on the cope surface. Few water modeling experiments have been conducted to correlate the pouring parameters and conditions to air entrainment during the pouring of metal castings. The results of the water modeling studies conducted by Wanstall et al. [10] and Bates and Griffin [11] showed that a throttled bottom pour ladle entrains significantly more air compared to an open nozzle (unthrottled) configuration. In addition, results from this study indicate that shorter falling heights and filling times

reduce the amount of entrained air. Through a series of experiments, Kuyucak [12] showed that using an offset pouring basin with a step before the sprue entrance allows the entrained air to escape to the atmosphere before entering the sprue. Additionally, it was found that the use of a nozzle extension submerged into the pouring basin significantly reduces the amount of entrained air during pouring. Afsharpour et al. [13] suggested that a conical pouring cup entrains large amount of bubbles, and using an offset step pouring basin and a small sprue reduces the air entrainment to a great extent.

Based on the work by Ma et al. [14], the authors have recently developed a model for predicting the local air entrainment rate [15]. The model accounts for the free surface turbulence at the liquid-air interface. The sub-grid model was implemented into a casting filling simulation code to calculate local air entrainment rates during filling. In the present study, the developed air entrainment model is validated by comparing the predicted relative air entrainment volumes with measured data from water modeling experiments [10,11]. It is shown how different pouring conditions, such as throttling the nozzle, nozzle diameter, head height, use of a nozzle extension for a bottom pour ladle, different pouring cup shapes, and tilted sprues, affect air entrainment.

2. Air Entrainment Model

This section describes the model for predicting the local air entrainment rate at free surfaces. The air entrainment calculations described here are performed as part of a standard casting filling simulation [16]. The filling simulation calculates the melt velocity and the geometry of the free surface at each time step.

Eddies in the turbulent flow raise disturbances on the periphery of the liquid jet, making the liquid-air interface rough (Figure 2). Air pockets are trapped inside these disturbances. Once air is entrained at the impact location, these air pockets are drawn into the bulk liquid where they are broken into smaller air bubbles and carried away with the liquid flow. In the developed model, the local air entrainment rate is a function of the turbulent kinetic energy, k, and the normal derivative of the normal component of the liquid velocity at the interface, $\partial u_n / \partial n$:

$$q = C_{ent} \frac{k}{g} \frac{\partial u_n}{\partial n} \qquad (1)$$

where q is the volumetric air entrainment rate per unit interfacial area, C_{ent} is the entrainment coefficient, and g (m s^{-2}) is the gravitational acceleration. The gradient term determines the possibility of air entrainment. A positive gradient term, $\partial u_n / \partial n > 0$, implies that the liquid velocity is increasing away from the interface, drawing the air pockets into the bulk liquid. On the other hand, for a negative gradient term, $\partial u_n / \partial n < 0$, the air pockets will be detrained rather than entrained. Therefore, the only scenario where air can be entrained is for positive values of $\partial u_n / \partial n$. In the developed model, the turbulent kinetic energy is estimated from the sum of the squares of the fluctuating velocity components relative to a spatially averaged mean velocity.
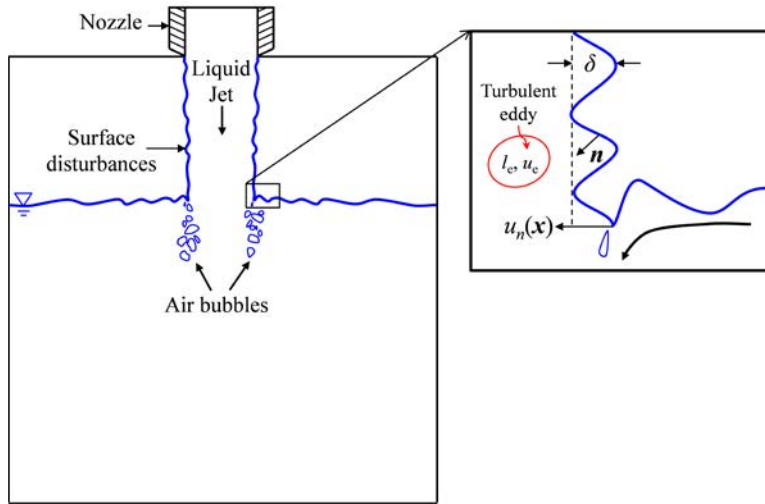
Figure 2. Surface disturbances along the periphery of a plunging liquid jet [15].

For calculating the volumetric air entrainment rate, Q_a (m³ s⁻¹), the air entrainment rate per unit interfacial area is integrated over the interfacial area, A_s

$$Q_a = \iint_{A_s} q \, \mathrm{d}A \qquad (2)$$

The entrainment coefficient, $C_{ent} = 0.039$, was estimated by calibrating the predicted relative air entrainment rates with the experimental measurements reported in [7] for plunging water jets with different liquid jet velocities, and diameters at low turbulence intensities. Calculation of the turbulent kinetic energy, the normal derivative of the normal component of the liquid velocity at the interface, and the calibration of the entrainment coefficient are explained in detail in a previously published paper by Majidi and Beckermann [15]. Using a single value of the air entrainment coefficient, a good agreement between measurements and predictions is achieved for plunging water jets with different liquid jet velocities, diameters and turbulence intensities.

3. Water Modeling Experiments

Water modeling experiments were conducted at the University of Alabama at Birmingham [10,11]. Water was poured using bottom pour, teapot, and quadrant ladles to study the effects of different variables on air entrainment.

Experimental Apparatus

For the bottom pour ladle trials, a 20" square by 26" deep acrylic ladle with an effective volume of approximately 4 ft³ was used (Figure 3a). The ladle had a hole at the bottom where nozzles of different diameters were inserted. The teapot ladle (Figure 3b) was a

4

commercial foundry ladle with an effective volume of 2.7 ft^3. Water exited the teapot ladle over a semi-circular shaped lip about 2.5" in diameter. A rotating potentiometer was mounted on the tilting axis of the teapot ladle for measuring the ladle rotation during pouring. The quadrant ladle, shown in Figure 3c, was made from 3/16" steel sheet with a back radius of 36" covering a 60° arc. The quadrant ladle's capacity was 4 ft^3, and had a rectangular lip with a width of 3.5" and a height of 2". The ladle was rotated around a steel rod that was supported on two ends. During pouring, a hoist raised a chain wrapped around the curved end of the ladle.

The tank into which water was poured consisted of an acrylic box with a height and width of 18" and a length of 36". Water was directly poured into the tank through the sprue. Water exiting the submerged sprue impinged on the quiescent water pool's surface. The water tank had a removable cover plate where sprues with different lengths and diameters could be inserted vertically or at an angle. The cover plate was sealed to the tank to prevent air leakage during pouring.
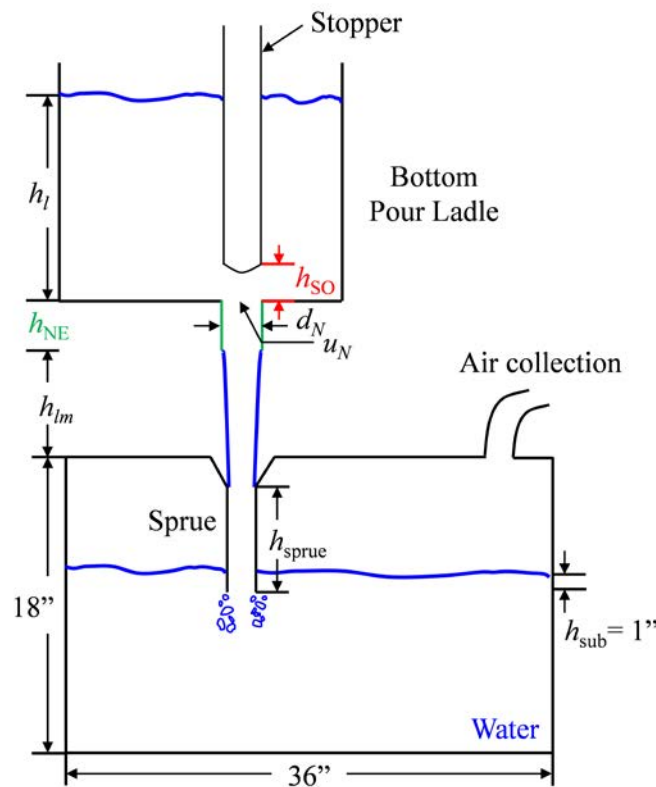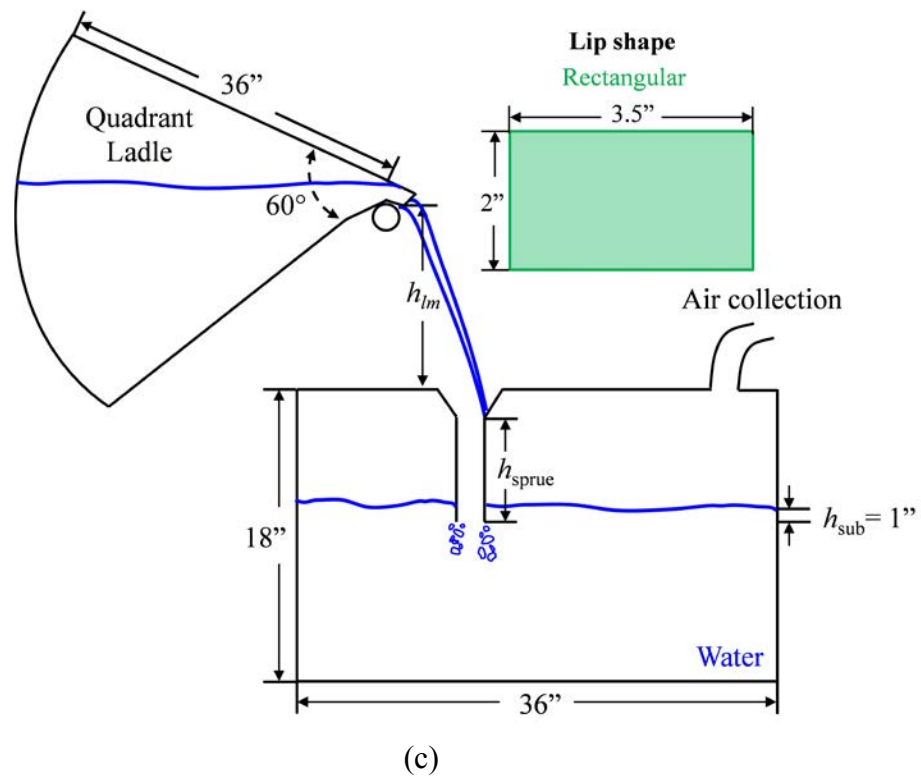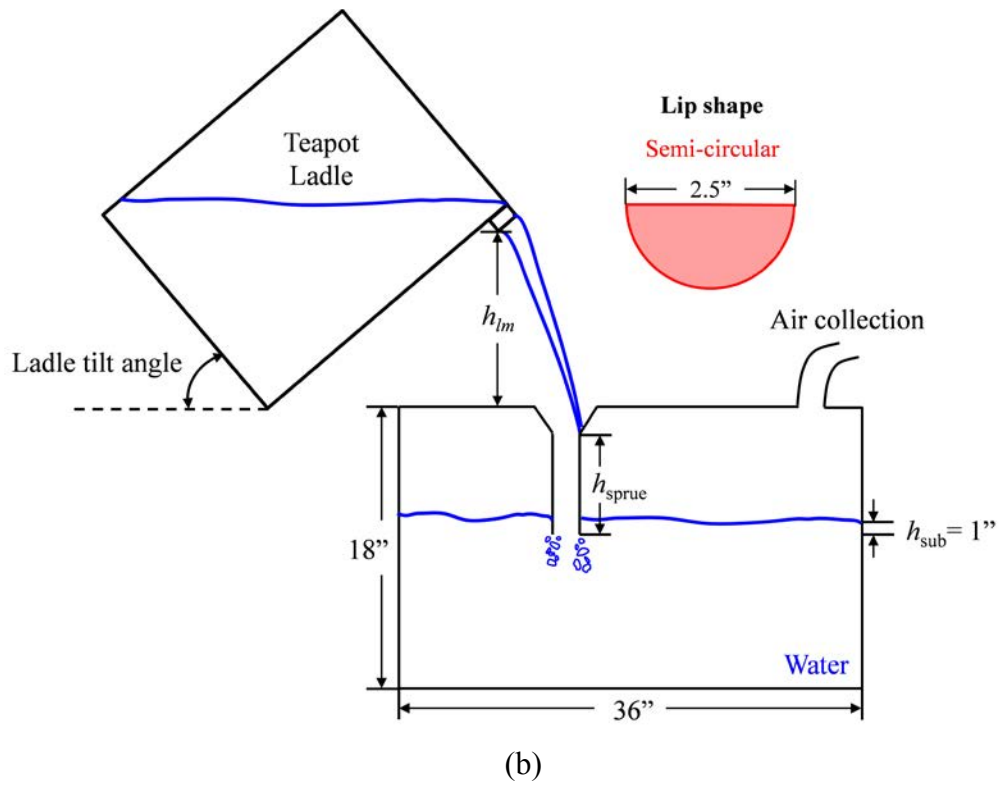

(a)

Figure 3. Experimental configuration for: (a) bottom pour ladle, (b) teapot ladle, and (c) quadrant ladle.

Measurements

The ladle weight was measured for each pour using a 1000 pound load cell attached to the ladle sling. Signals from the load cell, after amplification with a precision amplifier, were sent to a data acquisition board in a desktop computer. For each pour, the difference between the ladle weight at the beginning and at the end of the pour provided the total water poured.

For the bottom pour ladle, the pouring time was measured using an electronic switch, which was installed on the stopper lifting mechanism. The signals from the switch were sent to the data acquisition unit and the time difference between the start and end of each pour determined the pouring time. The electronic switch was manually controlled for the teapot and quadrant ladles.

Air is entrained when the water jet impinges on the quiescent pool surface. In addition to the entrained air, the impinging water caused some air displacement. The displaced and the entrained air were vented into a sealed bag at the top of the tank. At the end of the pouring, the bag was removed and the air inside was pumped through a gas flow meter to measure the total volume of collected air. The volume of entrained air was estimated as the difference between the total volume of collected air and the displaced air volume (determined form the volume of water poured). All the experimental results were expressed as the relative entrained air volume, i.e. the ratio of the entrained air volume to the volume of water poured. Based on the precision of measurement devices, the relative air entrainment precision was between 2% (at the higher air entrainment rates) and 12% (at the lowest observed rates).

Experimental Variables

A variety of pouring parameters were studied for each ladle. These parameters affect the velocity, diameter, falling height and the turbulence intensity of the liquid jet. For each parameter, a high and a low value were considered. The experiments were repeated three times for each configuration. For the bottom pour ladle, the effects of nozzle opening (open nozzle vs throttled nozzle), ladle depth, h_l, nozzle diameter, d_N, nozzle extension, h_{NE}, sprue length, h_{sprue}, were studied (Figure 3a). Table 1 lists all of the cases studied for the bottom pour ladle. The pouring times in Table 1 are the times for pouring 1 ft^3 of water. In all of the bottom pour ladle configurations, the distance between the ladle and the pouring cup was 3". The nozzle opening was controlled by changing the stopper opening height, h_{SO}, in Figure 3a. For the open nozzle configurations, h_{SO} = 2.5", and h_{SO} = 0.25" for the throttled configurations. To study the effect of total head height on the air entrainment, two different ladle depths and two sprue lengths were studied. For the full ladle and half-full ladle, the liquid height inside the ladle was 26" and 11", respectively. For the small nozzle diameter configurations (d_N = 1.88") a sprue diameter of d_{sprue} = 2" was used, while the sprue diameter was d_{sprue} = 3" for large nozzle diameter configurations (d_N = 2.56"). For all configurations with the nozzle extension, a h_{NE} = 5" extension with the same diameter as the nozzle was added to the nozzle exit. For this

7

purpose, the ladle was raised to maintain the height between the ladle and the pouring cup.

Table 1. Overview of the measured and simulated configurations for bottom pour ladle water modeling experiments.

	Trial	Ladle Depth	Nozzle Diameter (in)	Nozzle extension	Sprue Length (in)	Pouring time, t_{pour} (s)	Friction Coefficient, C_f (-)
Open Nozzle	1	Full	1.88	No	5.25	5.12	0.93
	2	Full	1.88	No	10.25	5.12	0.93
	3	Full	1.88	Yes	5.25	5.68	0.85
	4	Full	1.88	Yes	10.25	5.67	0.85
	5	Full	2.56	No	5.25	3.91	0.68
	6	Full	2.56	No	10.25	3.91	0.68
	7	Half-full	1.88	No	5.25	8.37	0.99
	8	Half-full	1.88	No	10.25	8.36	0.99
	9	Half-full	1.88	Yes	5.25	9.17	0.93
	10	Half-full	1.88	Yes	10.25	9.17	0.93
	11	Half-full	2.56	No	5.25	6.22	0.78
	12	Half-full	2.56	No	10.25	6.25	0.78
Throttled Nozzle	13	Full	1.88	No	5.25	12.2	0.48
	14	Full	1.88	No	10.25	12.2	0.48
	15	Full	1.88	Yes	5.25	10.0	0.52
	16	Full	1.88	Yes	10.25	9.95	0.52
	17	Full	2.56	No	5.25	7.9	0.42
	18	Full	2.56	No	10.25	7.85	0.42
	19	Half-full	1.88	No	5.25	21.2	0.59
	20	Half-full	1.88	No	10.25	20.6	0.60
	20	Half-full	1.88	Yes	5.25	16.4	0.64
	22	Half-full	1.88	Yes	10.25	18.5	0.61
	23	Half-full	2.56	No	5.25	13.8	0.60
	24	Half-full	2.56	No	10.25	13.9	0.60

For the teapot ladle, the effects of ladle depth (ladle tilt angle), pouring basin (impact surface), sprue tilt, and sprue length were studied (Figure 3b). For the full ladle and half-full ladle configurations, the ladle was tilted from 0 degree, and 40 degrees, respectively. The air entrainment was also measured for two different pouring cups, a conical cup and a half-cone cup. For the configurations with tilted sprue, the sprue was tilted 30° from its vertical position. Two different sprue heights were also studied. The distance between the teapot ladle lip and the cup was sufficiently high to pour 1 ft³ of water before the ladle lip touched the cup (approximately 2").

For the quadrant ladle (Figure 3c), a full and half-full ladle configuration with a short and tilted sprue were tested to compare with the results of the teapot ladle under similar conditions. Table 2 lists all of the cases studied for the teapot and quadrant ladles. More details of the experiments can be found in References [10,11].

8

Table 2. Overview of the measured and simulated cases for the teapot and quadrant ladles.

	Trial	Ladle Depth	Pouring cup	Sprue Tilt Angle (°)	Sprue Length (in)	Pouring time, t_{pour} (s)
Teapot Ladle	1	Full	Conical	0	5.25	30.0
	2	Full	Conical	0	10.25	30.3
	3	Full	Conical	30	5.25	31.6
	4	Full	Conical	30	10.25	34.4
	5	Full	Half-cone	0	5.25	28.5
	6	Full	Half-cone	0	10.25	29.6
	7	Half-full	Conical	0	5.25	27.9
	8	Half-full	Conical	0	10.25	26.6
	9	Half-full	Conical	30	5.25	31.4
	10	Half-full	Conical	30	10.25	36.2
	11	Half-full	Half-cone	0	5.25	28.5
	12	Half-full	Half-cone	0	10.25	31.9
Quadrant Ladle	13	Full	Conical	30	5.25	35.4
	14	Half-full	Conical	30	5.25	33.2

4. Simulation of Water Modeling Experiments

The developed air entrainment model was applied to the water modeling studies explained at section 3. For reducing the simulation time a smaller water tank was utilized; the height and width (18") were the same as the height and width of the water tank used in the above experiments, while the length of the tank was reduced from 36" to 26" (Figure 4 and Figure 5) for the simulations. However, the tank size was sufficiently large that the boundaries had no influence on the impact location at the water pool surface, where air entrainment occurs. Similar to the experiments, in all configurations the sprue was submerged approximately 1" into the water. For all the bottom pour, teapot, and quadrant ladle cases, instead of modeling the ladles, the volumetric flow rate of water was calculated and used as the input for the simulations. The thermo-physical properties of water were used in the simulations.

Bottom Pour Ladle

Using the simplified energy conservation equation (Equation 3), i.e. Bernoulli equation, and the continuity equation (Equation 4), an equation was derived for the liquid velocity at the nozzle exit, $u_{N,th}$:

$$u_{N,th} = \sqrt{2gh_l(t)} \tag{3}$$

$$-\frac{dh_l}{dt} \times A_{ladle} = A_N \times u_{N,th} \tag{4}$$

$$u_{N,th}(t) = 27.8h_{l,i}^{\frac{1}{2}} - 386.1\frac{A_N}{A_{ladle}}t \tag{5}$$

where h_l (in) and $h_{l,i}$ (in) are the instantaneous and initial water height inside the bottom pour ladle, respectively, and A_N (in²) is the nozzle cross sectional area

$$A_N = \frac{\pi}{4}d_N^2 \tag{6}$$

Based on the effective volume, V_{ladle} = 4 ft³, and height of the bottom pour ladle, h_{ladle} = 26", an equivalent ladle cross-sectional area was calculated as $A_{ladle} = V_{ladle} / h_{ladle}$ = 266 in².

(a)   (b)
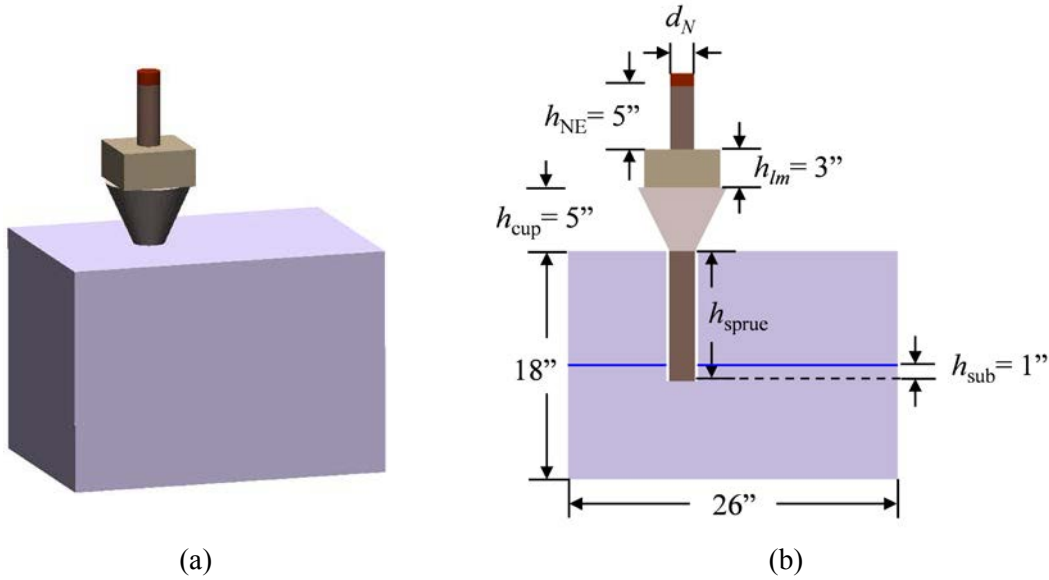
Figure 4. Simulation configuration (a) isometric view, and (b) mid-plane view showing parameters studied for the bottom pour ladle: Effects of nozzle diameter, d_N, sprue height, h_{sprue}, and nozzle extension, h_{NE}.

In the simulations, a friction coefficient, C_f, was applied to the liquid velocity at the nozzle exit to account for the nozzle friction. The effective liquid velocity, $u_{N,eff}$, and volumetric flow rate, Q_w, at the nozzle exit were calculated as

$$u_{N,eff}(t) = C_f \times u_{N,th}(t) \tag{7}$$

$$Q_w(t) = \frac{\pi}{4} d_N^2 u_{N,eff}(t) \tag{8}$$

To estimate the friction coefficient, first, the total volume of water poured was calculated by integrating the volumetric flow rate, Q_w, over the pouring time, t_{pour}

$$V_w = \int_0^{t_{\text{pour}}} Q_w(t)dt = \frac{\pi}{4} d_N^2 \times C_f \int_0^{t_{\text{pour}}} u_{N,th}(t)dt \tag{9}$$

Then, based on the reported pouring time for 1 ft^3 of water, the friction coefficient, C_f, was calculated for each configuration. The calculated friction coefficients are shown in Table 1. The further a friction coefficient is below unity, the more friction is present in a nozzle.

According to the experimental observations of the throttled nozzle, the liquid at the nozzle exit had a large turbulence level. To model the throttled nozzle configurations, turbulence intensity was applied at the nozzle exit in the simulations. The turbulence intensity indicates the level of fluctuations in a turbulent flow and is defined as

$$I = \frac{\sqrt{\overline{u'^2_{N,eff}}}}{\overline{u_{N,eff}}} \tag{10}$$

where the prime and the overbar indicate the fluctuating and mean components of the liquid velocity at the nozzle exit, respectively. By applying turbulence intensity, the volumetric flow rate of water at the nozzle exit was calculated as

$$Q_w(t) = \frac{\pi}{4} d_N^2 u_{N,\text{eff}} \left[1 + I \times \sin(\pi \times f \times t) \right] \tag{11}$$

where f and t are the frequency of the fluctuations and time, respectively. To determine the turbulence intensity, two configurations: full ladle, long sprue, no nozzle extension, with small and large nozzle diameters, were simulated with different turbulence levels and compared with the experimental measurements. Finally, a turbulence intensity of $I = 70\%$ and frequency of $f = 10$ Hz were selected for all of the throttled cases. Simulation results indicate that the relative air entrainment volumes are independent of frequency in the range of $5 \leq f(\text{Hz}) \leq 15$. Zero turbulence level ($I = 0$) was applied for all of the open nozzle cases.

The large turbulence intensity at the nozzle exit generated large disturbances at the periphery of the liquid jet. The disturbances hitting the bottom of the pouring cup blocked the flow from entering to the sprue. This caused the water to overflow from the cup before the sprue was filled during the simulations for the small nozzle diameter configurations. Therefore, for the throttled small nozzle configurations, a sprue with slightly larger diameter, $d_{\text{sprue}} = 2.5$", and a pouring cup with larger diameter was used in the simulations. Water did not overflow the cup in the simulations of the throttled large nozzle diameter cases; therefore, the diameter of the sprue and pouring cup was not changed for these configurations. Similar to the experiments, for all the bottom pour ladle

11

trials the stream was centered above the sprue. For each of the open and throttled nozzles, the effects of ladle depth, nozzle diameter, sprue length, and nozzle extension were studied (Figure 4 and Table 1).

Teapot and Quadrant ladles

For the teapot and quadrant ladle cases, based on the reported volume of water poured, V_w, and the pouring time from the experiments, t_{pour}, an average pouring rate was calculated for each configuration and used as the input for simulations:

$$Q_w = \frac{V_w}{t_{pour}} \tag{12}$$

The effects of ladle depth (ladle tilt angle), pouring cup type, sprue tilt, and sprue length were studied for the teapot ladle (Figure 5 and Table 2). The effect of ladle tilt angle was simulated by changing the θ_{tilt} in Figure 5; for the full ladle configurations, a small tilt angle ($\theta_{tilt} = 15°$), and for half-full ladle cases a relatively larger tilt angle ($\theta_{tilt} = 35°$) in the simulations.

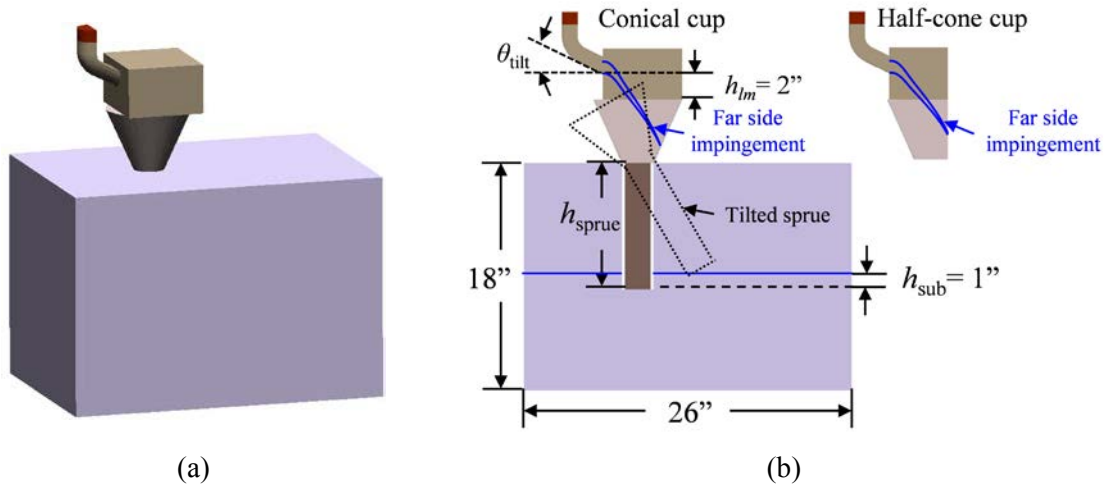(a)   (b)

Figure 5. Simulation configuration (a) isometric view, and (b) mid-plane view showing parameters studied for the teapot ladle: Effects of ladle tilt angle, θ_{tilt}, pouring cup, sprue tilt and sprue height, h_{sprue}.

For the tilted sprue cases, the sprue and the pouring cup were tilted 30° from the vertical position. The quadrant ladle and teapot ladle simulation setups were similar, except that a semi-circular lip, was used for the teapot ladle (Figure 3b), and a rectangular lip (Figure 3c) was used for the quadrant ladle simulations. For the simulation of teapot and quadrant ladle configurations, the distance between the ladle lip and cup was kept constant ($h_{lm} = 2$") during pouring. It was assumed that stream exiting the lip of the teapot and quadrant ladles impinged on the far side of the cup surface (Figure 5b) before entering the sprue.

5. Results and Discussion

Before comparing the predicted results to the measurements for different configurations, a computational mesh dependency study was performed for the base case (bottom pour ladle, open nozzle, half-full ladle, small nozzle diameter, long sprue, and no nozzle extension). In all cases, a uniform mesh was utilized that consists of cubes of a certain side length. Figure 6 shows that as the grid spacing is refined from a 7.3 mm to a 3.6 mm, the predicted relative air entrainment volume, V_a / V_w, experiences a slight change, though the total metal cells increase from 400000 to 3200000. This relatively minor mesh dependency is acceptable. For all of the following configurations a uniform grid spacing of 6.3 mm is used.
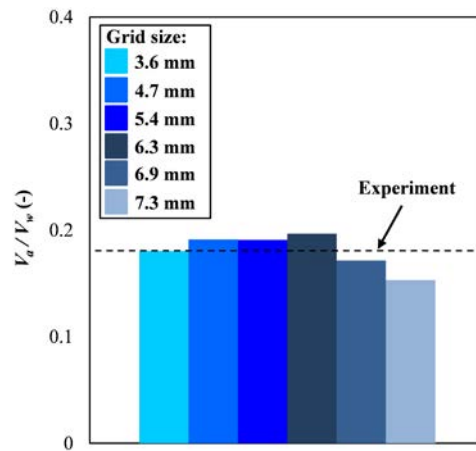

Figure 6. Predicted relative air entrainment rate volume as a function of grid spacing for the bottom pour ladle, open nozzle, half-full ladle, small nozzle diameter ($d_N = 1.88$"), long sprue ($h_{\text{sprue}} = 10.25$") and no nozzle extension configuration.

Figure 7 shows the local air entrainment rate of the base configuration. As expected, the predicted volumetric air entrainment rate shows that the air entrainment takes place at the periphery of the liquid jet where it plunges into the quiescent pool.
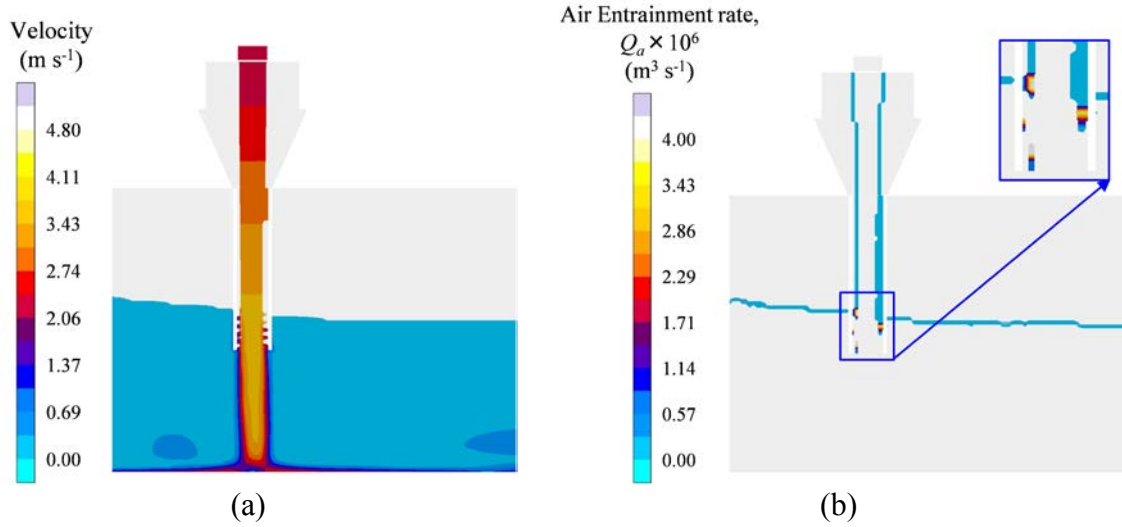
Figure 7. Contours of (a) velocity, and (b) volumetric air entrainment rate, Q_a, at $t = 2$ s for the bottom pour ladle, open nozzle, half-full ladle, small nozzle diameter ($d_N = 1.88$"), long sprue ($h_{sprue} = 10.25$") and no nozzle extension configuration.

Bottom Pour Ladle

Figure 8 shows the predicted relative air entrainment rate for two ladle depths. The comparison is made for the open nozzle, small nozzle diameter, long sprue, and no nozzle extension case. Once the liquid jet impinges into the water pool, air is entrained at the impact location. The large initial spike is due to the initial impact of the liquid jet on the water pool; this spike is larger for the full ladle configuration. A larger head height of liquid inside the ladle implies more hydrostatic pressure above the nozzle, and a consequently, a larger liquid velocity at the nozzle exit. A higher liquid velocity at the nozzle exit results in a higher liquid jet velocity at impact location, which leads to a higher air entrainment rate. After the initial spike, the relative air entrainment decreases as the water tank is filled. The decrease is more pronounced for the full ladle since the water tank is filled faster than the half-full ladle case. As mentioned earlier, zero turbulence intensity is applied at the nozzle exit for the open nozzle configurations. Therefore, the fluctuations during this period are generated due to unsteadiness of the flow.
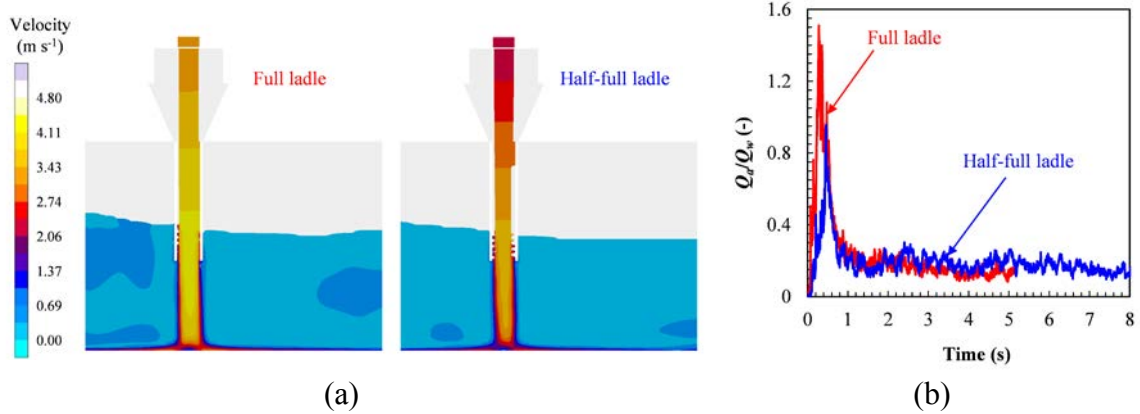
14

(a)　　　　　　　　　　　　　　　　(b)

Figure 8. Effect of the ladle depth on the variation of the relative air entrainment rate for open stopper, small nozzle diameter ($d_N = 1.88$"), long sprue ($h_{sprue} = 10.25$") and no nozzle extension configuration: (a) The velocity contours at time of $t = 2$ s for full ladle (left) and half-full ladle (right), and (b) relative air entrainment rate.

Figure 9 compares the air entrainment predictions for the open nozzle and throttled nozzle. The comparison is made for the full ladle, small nozzle diameter, long sprue and no nozzle extension configurations. Throttling the nozzle increases the turbulence intensity of the liquid jet at the nozzle exit, which increases the size of the disturbances on the periphery of the liquid jet, thereby increasing the air entrainment rate at the impingement point. Throughout the pouring, the air entrainment rate is significantly larger for the throttled nozzle than for the open nozzle configuration.
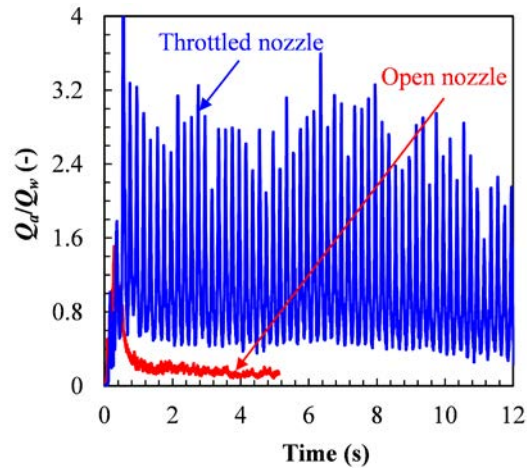

Figure 9. Effect of the nozzle opening on the variation of the relative air entrainment rate for full ladle, small nozzle diameter ($d_N = 1.88$"), long sprue ($h_{sprue} = 10.25$") and no nozzle extension configuration.

Figure 10 compares the total volume of entrained air per volume of water poured for all open (Figure 10a) and throttled (Figure 10b) bottom pour ladle cases. The standard deviations in Figure 10 are calculated based on the three measured relative air

15

entrainment volumes for each configuration. The comparison between the predicted values and experimental measurements shows overall excellent agreement. However, some discrepancies can be observed for the throttled cases. The standard deviation for the experimental results indicate that the throttled configurations have the largest variations in the measurements. Moreover, some of the measurement results of the throttled configurations contradict previous findings of different experiments. For example, an increase in the sprue length reduces the air entrainment for the full ladle, large nozzle diameter and also for the half-full ladle, small nozzle diameter without nozzle extension cases. The authors believe that the complex behavior of the throttling process cannot be solely modeled by applying a single turbulence intensity at the nozzle exit. In addition, a throttled nozzle reduces the effective nozzle cross sectional area, which has not been accounted for in the simulations.

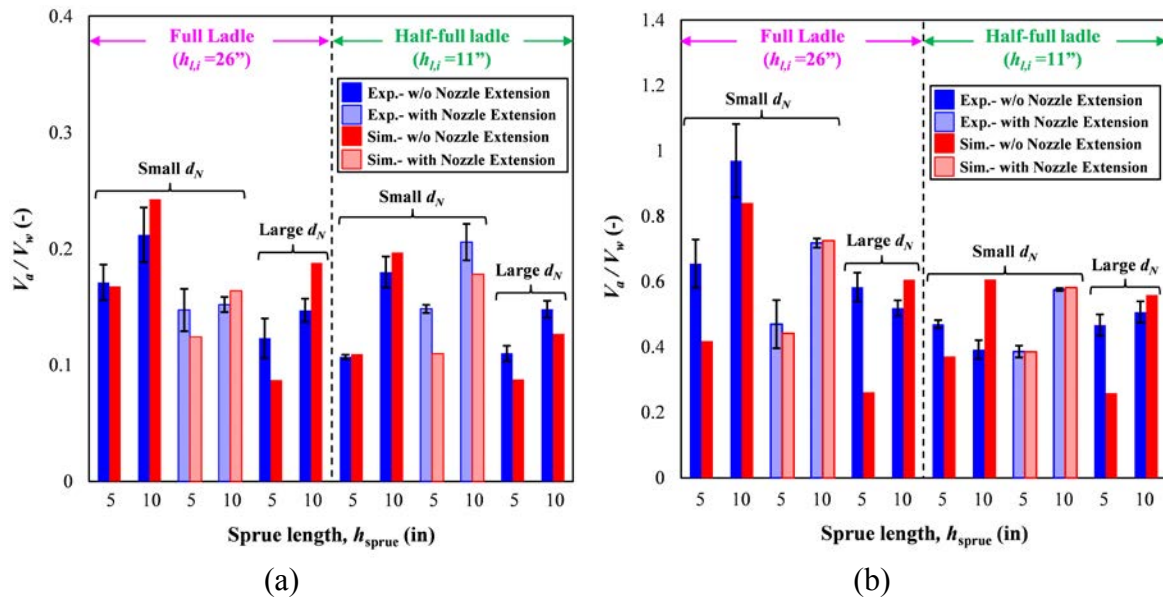(a)   (b)

Figure 10. Comparison of the predicted relative entrained air volumes with measurements for 24 bottom pour ladle configurations: (a) open nozzle, and (b) throttled nozzle.

Comparing Figures 10a and 10b, the throttled nozzle configurations entrain significantly more air than the open nozzle. Throttling the nozzle reduces the liquid velocity at the nozzle exit; this is shown through the decrease in the friction coefficient in Table 1. On the other hand, the large turbulence intensity applied at the nozzle exit for the throttled cases increases the disturbance size on the periphery of the plunging liquid jet; hence, the rise in air entrainment. Figure 10b indicates the effect of increased turbulence intensity outweighs the effect of reduced liquid jet velocity. Throttling the nozzle results in relative entrained air as high as 1 cubic foot of air per cubic foot of liquid poured. Obviously, the turbulence level of the plunging liquid jet has a significant effect on the air entrainment.

The results also show that due to the larger velocity at the nozzle exit, the full ladle configurations entrain more air than the half-full ladle cases.

Comparison between the small nozzle diameter and large nozzle diameter configurations indicates that increasing the diameter of the stream emanating from the ladle reduces the relative air entrainment volume. A larger nozzle diameter produces a higher flow rate, and a higher flow rate reduces the filling time. Additionally, according to Table 1, the nozzle friction is greater for the large nozzle diameters than the small nozzle diameters. This results in even smaller water jet velocities at the nozzle exit for the large nozzle diameter cases, which further reduces the air entrainment.

Figure 10 also shows that increasing the falling height of the impinging water from the nozzle increases the relative air entrainment volume. A longer sprue implies a larger falling height, which increases the water jet velocity at the impact location and, hence, the volume of entrained air.

The nozzle extension affects the open nozzle and throttled nozzle cases differently. For the open nozzle configurations, adding an extension to the exit of the nozzle applies more friction to the plunging liquid jet. The calculated friction coefficients, presented in Table 1, reflect this fact. This reduces the velocity of the stream exiting the nozzle extension and, therefore, the air entrainment. For the throttled nozzle cases, the addition of a nozzle extension reduces the effect of turbulence intensity. This is because the walls of the nozzle extension eliminate the free surface disturbances on the periphery of the liquid jet, which are generated at the nozzle exit before the extension; this in turn reduces the air entrainment. On the other hand, for both the open and throttled configurations, when a nozzle extension was used, the ladle was raised to maintain the height of the free falling jet. This increases the velocity of the liquid at the exit of the extension, which increases air entrainment. Therefore, the impact of the lower velocities due to an increase in nozzle friction for the open nozzle configurations and the reduction of turbulence intensity for the throttled cases, are reduced by the effect of higher velocities at the jet impingement point caused by the increase in total head height. The simulation results, in Figure 10, show that the relative air entrainment volume is larger for the configurations without a nozzle extension.

It is important to point out that the open nozzle configuration with half-full ladle, large nozzle diameter, and short sprue entrains the least amount of air. A comparison of the 24 bottom pour ladle configurations shows that the amount of entrained air differs by a factor of nearly 10 between the cases with least and most entrained air.

Teapot and Quadrant Ladles

Figure 11 compares the relative air entrainment rate for two different ladle depths (ladle tilt angles) for the conical cup, vertical and long sprue configuration. The results indicate that increasing the tilt angle reduces the relative air entrainment rate, though the difference is rather small. Therefore, by assuming a constant pouring rate and that the water jet impinges on the far side of the pouring cup for both configurations, the ladle tilt angle does not significantly affect the air entrainment. According to Figure 11b, as the water tank fills, the relative air entrainment decreases due to the continuous decrease in total head height.

17

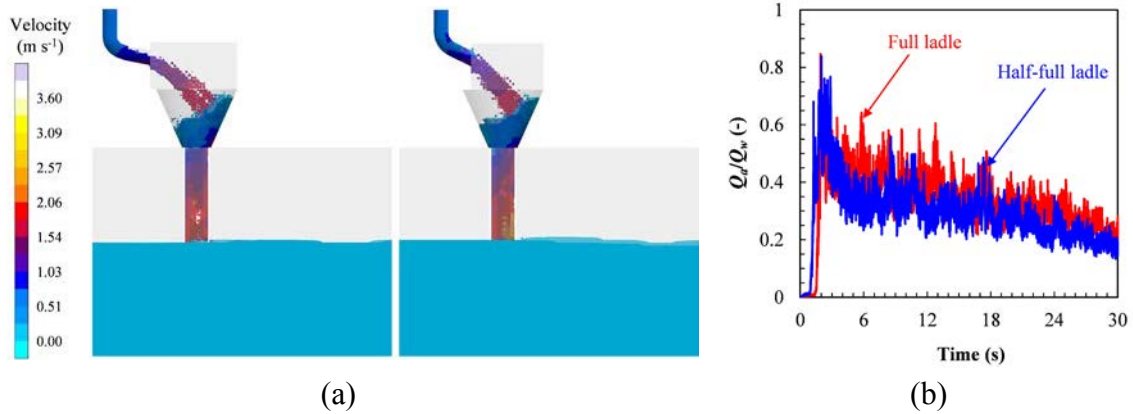(a)   (b)

Figure 11. Effect of the ladle depth (ladle tilt angle) on the variation of the relative air entrainment rate for the conical cup, vertical and long sprue ($h_{sprue} = 10.25$") teapot ladle configuration: (a) The velocity contours at time of $t = 6$ s for full ladle (left) and half-full ladle (right), and (b) relative air entrainment rate.

Figure 12 compares the measured and predicted relative entrained air volume for all different teapot ladle configurations. While the pouring cup, the sprue tilt and length have a great effect on the air entrainment, the ladle depth (ladle tilt angle) effect on the air entrainment is negligible. Results show that the half-cone configurations entrain more air than the conical pouring cup cases. This difference is more pronounced for the longer sprue configurations. For the water jet impinging on the round conical cup surface, the flow slides on the cup surface before entering the sprue. However, for the half-cone cup, after water impinges on the flat cup surface, it enters directly into the sprue. Predicted results also indicate that a tilted sprue entrains less air compared to a vertical sprue. Tilting the sprue from the vertical position reduces the effective total head height, the distance between the ladle lip and the water pool surface. Similar to the bottom pour ladle configurations, due to a larger falling height for a longer sprue, increasing the sprue length significantly increases the relative entrained air volume. Comparison between experimental measurements and simulated predictions indicates an overall good agreement. The only significant disagreement between the measured and predicted values is for the full ladle and half-cone cup, where the measurements indicate that increasing the sprue length reduces the relative air entrainment. This disagrees with the previous conclusions regarding the total falling height for the bottom pour and teapot ladle cases.
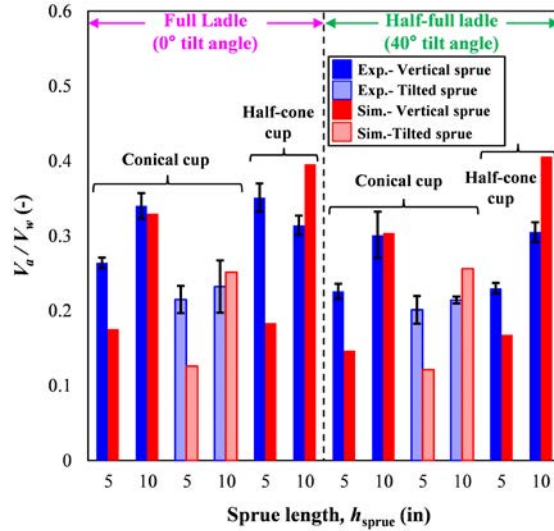
Figure 12. Comparison of the predicted relative entrained air volumes with measurements for the 12 teapot ladle configurations.

An increased lip cross-sectional area for the quadrant ladle compared to the teapot ladle reduces slightly the predicted relative air entrainment (Figure 13). Similar to the teapot ladle configurations, the quadrant ladles' predicted relative air entrainment does not significantly change for different ladle depths (ladle tilt angles). Though comparing the measured results of teapot and quadrant ladle configurations shows that the ladle type significantly affects the relative air entrainment, the predicted results contradict this conclusion (Figure 13). This could be due to the differences in the distance between the lip and pouring cup for the two ladles. In addition, this variation could also arise due to the difference between impingement points of the water on the pouring cup for quadrant and teapot ladle configurations. As mentioned earlier, in the simulations the drop height (distance between the lip and pouring cup) and the impingement point are kept the same for the teapot and quadrant ladles. However, in reality, keeping the ladle height and the plunging point constant is almost impossible during pouring of liquids.

Comparison of Bottom Pour and Teapot Ladles

Figure 14 compares the average of the experimental measurements and predicted relative air entrainment of the bottom pour and teapot ladle cases. Since only two configurations were studied for the quadrant ladle, the average values of the quadrant ladle cases are not presented here. An excellent agreement is obtained between the average measured and predicted relative air entrainment volumes. The results indicate that throttled nozzle configurations entrain significantly more air than the open nozzle and teapot ladle configurations. For the bottom pour ladle, throttling the nozzle can increase the entrained air by more than three times. Therefore, the turbulence level of the liquid at the ladle exit has the most notable effect on the air entrainment. The calculated standard deviations for each ladle type, shown in Figure 14, demonstrate the throttled nozzle configurations have the largest variations in the measurements and predictions.
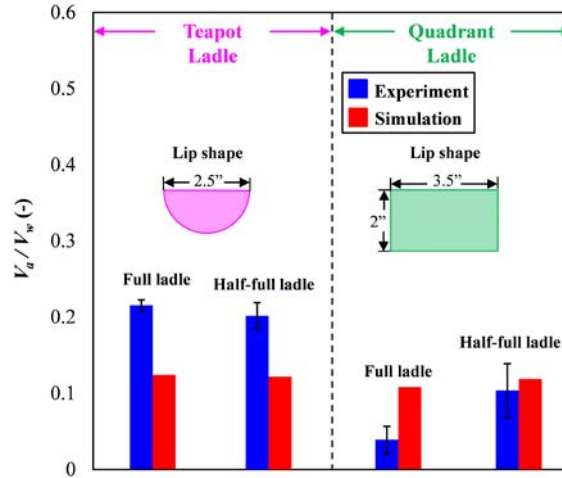
Figure 13. Comparison of the teapot and quadrant ladles for the short ($h_{\text{sprue}} = 5.25\text{''}$) and tilted sprue (30° tilt).
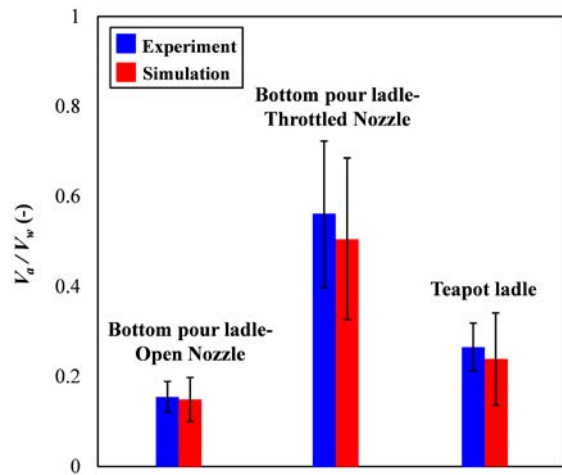

Figure 14. Comparison of the average predicted and measured total relative entrained air volumes for bottom pour and teapot ladle configurations.

5. Conclusion

The air entrainment model recently developed by the authors is validated for water modeling experiments. Overall good agreement is achieved between the predicted and the measured relative air entrainment volumes. Results indicate that reducing the total head height and adding a nozzle extension to the end of the nozzle reduces the air entrainment during filling. In addition, increasing the nozzle diameter increases the volumetric water flow rate, which reduces the pouring time and therefore, the entrained air volume. The nozzle opening has the most significant effect upon the air entrainment. A throttled nozzle applies large turbulence intensity to the flow at the nozzle exit, markedly increasing the air entrainment volume. Clearly, producing clean castings requires the

nozzle to be fully opened during pouring. It is also found that for a constant pouring rate and ladle to mold distance, the teapot ladle tilt angle does not affect the air entrainment significantly. The promising results obtained in this study further validate the developed air entrainment model.

Future work will link the present air entrainment model to an inclusion generation and transport model, where the final reoxidation inclusion size and location can be predicted.

Acknowledgments

References

1.   A.J. Melendez, K.D. Carlson and C. Beckermann, "Modelling of Reoxidation Inclusion Formation in Steel Casting", *International Journal of Cast Metal Research*, 2009, Vol. 32, pp. 624-638.
2.   T.J. Lin and H.G. Donnelly. "Gas bubble entrainment by plunging laminar liquid jets." *AIChE Journal*, 1966, Vol. 12, pp. 563-571.
3.   A.K. Biń. "Gas entrainment by plunging liquid jets" *Chemical Engineering Science*, 1993, Vol. 48, pp. 3585-3630.
4.   D.A. Ervine, E. McKeough and E.M. Elsawy, "Effect of Turbulence Intensity on the Rate of Air Entrainment by Plunging Water Jets", *ICE Proceedings*, 1980, Vol. 69, pp. 425-445.
5.   D. Mouaze, F Murzyn and J.R. Chaplin, "Free Surface Length Scale Estimation in Hydraulic Jumps", *Journal of Fluids Engineering*, 2005, Vol. 127, pp. 1191-1193.
6.   K.T. Kiger and J.H. Duncan, "Air Entrainment Mechanisms in Plunging Jets and Breaking Waves", *Annual Review of Fluid Mechanics*, 2012, Vol. 44, pp. 563-596.
7.   K.J. Sene, "Air Entrainment by Plunging Jets", *Chemical Engineering Science*, 1988, Vol. 43, pp. 2615-2623.
8.   E. Van de Sande and J.M. Smith, "Jet break-up and air entrainment by low velocity turbulent water jets", *Chemical Engineering Science*, 1976, Vol. 31, pp. 219-224.
9.   T. Brattberg and H. Chanson, "Air entrapment and air bubble dispersion at two-dimensional plunging water jets", *Chemical Engineering Science*, 1998, Vol. 24, pp. 4113-4127.
10.   C. Wanstall, J. Griffin and C.E. Bates, "Water Modeling of Steel Pouring Practices", Proc. 47th SFSA Technical and Operating Conference, Paper No. 1.1, Chicago, IL, 1993.
11.   C.E. Bates and J. Griffin, "Clean Cast Steel Technology", Research report no. 106, Steel Founders' Society of America (SFSA), Crystal Lake, IL, USA, 1994.
12.   S. Kuyucak, "Sponsored Research: Clean steel casting production- Water modeling studies of bottom-pouring ladle operations", *AFS Trans.*, 2006, Vol. 114, pp. 811-818.

13.   M. Afsharpour, B. Homayun and S.M.A. Boutorabi, "Water Modelling of effects of pouring basin and sprue geometry on entrance of air bubbles into mould", *Materials Science and Technology*, 2014, Vol. 30, pp. 152-159.

14.   J. Ma, A.A. Oberai, D.A. Drew, R.T. Lahey and M. Hyman, "A Comprehensive Sub-Grid Air Entrainment Model for RANS Modeling of Free- Surface Bubbly Flows", *Journal of Computational Multiphase Flow*, 2011, Vol. 3, pp. 41-56.

15.   S.H. Majidi and C. Beckermann, "Modelling of air entrainment during pouring of metal castings", *International Journal of Cast Metal Research*, 2017, Vol. 30, pp. 301-315.

16.   *MAGMAsoft*, MAGMA Gmbh, Kackerstrasse 11, 52072 Aachen, Germany.